

Relaxed random walks at scale

ALEXANDER A. FISHER¹,
XIANG JI¹,
PHILIPPE LEMEY²,
AND MARC A. SUCHARD^{1,3,4}

¹*Department of Biomathematics, David Geffen School of Medicine at UCLA, University of California, Los Angeles, United States*

²*Department of Microbiology and Immunology, Rega Institute, KU Leuven, Leuven, Belgium*

³*Department of Biostatistics, Jonathan and Karin Fielding School of Public Health, University of California, Los Angeles, United States*

⁴*Department of Human Genetics, David Geffen School of Medicine at UCLA, University of California, Los Angeles, United States*

Corresponding author: Marc A. Suchard, Departments of Biostatistics, Biomathematics, and Human Genetics, University of California, Los Angeles, 695 Charles E. Young Dr., South, Los Angeles, CA 90095-7088, USA; E-mail: msuchard@ucla.edu

Abstract Relaxed random walk (RRW) models of trait evolution introduce branch-specific rate multipliers to modulate the variance of a standard Brownian diffusion process along a phylogeny and more accurately model overdispersed biological data. Increased taxonomic sampling challenges inference under RRWs as the number of unknown parameters grows with the number of taxa. To solve this problem, we present a scalable method to efficiently fit RRWs and infer this branch-specific variation in a Bayesian framework. We develop a Hamiltonian Monte Carlo (HMC) sampler to approximate the high-dimensional, correlated posterior that exploits a closed-form evaluation of the gradient of the trait data log-likelihood with respect to all branch-rate multipliers simultaneously. Remarkably, this gradient calculation achieves computational complexity that scales only linearly with the number of taxa under study. We compare the efficiency of our HMC sampler to the previously standard univariable Metropolis-Hastings approach while studying the spatial emergence of the West Nile virus in North America in the early 2000s. Our method achieves an over 300-fold speed-increase over the univariable approach. Additionally, we demonstrate the scalability of our method by applying the RRW to study the correlation between mammalian adult body mass and litter size in a phylogenetic tree with 2306 tips.

1 Introduction

Phylogenetic comparative methods are an indispensable tool to study the evolution of biological traits across taxa while controlling for their shared evolutionary history that confounds the inference of trait correlation (Felsenstein, 1985). Modern comparative methods usually entertain continuous, multivariate traits, although extensions to mixed discrete and continuous outcomes are readily available (Cybis *et al.*, 2015; Ives and Garland Jr, 2009). Approaches typically model trait evolution as a Brownian diffusion or “random walk” process that acts conditionally independently along the branches of a known or random phylogeny. Specifically, the observed or latent trait value of a node in a phylogeny arises from a multivariate normal distribution centered on the latent trait value of its ancestral node with variance proportional to the units of time between nodes. A strict Brownian diffusion model, however, is unable to accommodate the overdispersion in trait data that often emerges from real biological processes (Schluter *et al.*, 1997). One such example arises when examining the dispersal rate of measurably evolving viral pathogens (Biek *et al.*, 2007). For example, if birds serve as the viral host, migratory patterns may induce inhomogeneous dispersal rates over time (Pybus *et al.*, 2012). In such cases, a strict Brownian diffusion model fails to capture, and therefore can also fail to predict, the spatial dynamics of an emerging epidemic.

Lemey *et al.* (2010) relax the strict Brownian diffusion assumption by introducing branch-rate multipliers that scale the variance of the Brownian diffusion process along each branch of the phylogeny. This “relaxed random walk” (RRW) model requires estimating $2N - 2$ correlated branch-rate multipliers, where N is the number of taxa in the phylogeny. Lemey *et al.* (2010) take a Bayesian approach to parameter estimation where they infer the posterior distribution of the branch-rate multipliers via Markov chain Monte Carlo (MCMC) employing a simple univariable Metropolis-Hastings (UMH) proposal distribution (Hastings, 1970). Since the rates remain correlated in the posterior, a random-scan (Liu, 2008) of UMH proposals inefficiently explores branch-rate space. Specifically, univariable samplers

force accepted proposals to be very close together to avoid a large number of rejection steps in the Markov chain simulation. This results in high correlation between MCMC samples from the posterior, making point estimates of the branch-rate multipliers unreliable and slow to converge. Despite these drawbacks, RRWs find many impactful applications, e.g., in phylodynamics and phylogeography (Bedford *et al.*, 2014; Faria *et al.*, 2014).

To ameliorate the difficulties that high dimensional MCMC sampling presents, we propose adopting a geometry-informed sampling approach using Hamiltonian Monte Carlo (HMC). HMC equates sampling from a probability distribution with simulating the trajectory of a puck sliding across a frictionless surface warped by the shape of the distribution (Neal, 2011). To map from this statistical problem to the physical one, we view the MCMC samples of our branch-rate multipliers as the “position” of the puck and, then, for each positional dimension we introduce an associated momentum variable. In this way, we extend a D-dimensional parameter space to 2D-dimensional phase space (Betancourt, 2017) and traverse the 2D phase space via differentiating the Hamiltonian and using a numerical integration method to offer proposal states for our MCMC chain. The major limitation to HMC is calculating the gradient of the log-posterior with respect to all position parameters simultaneously. Previous approaches for calculating gradients on phylogenies have employed “pruning”-type algorithms (Felsenstein, 1981) that scale quadratically with the number of taxa in the tree (Bryant *et al.*, 2005). Likewise, numerical approaches also scale quadratically.

In this paper, we derive a method to calculate the gradient with computational complexity that scales only linearly with the number of taxa. We implement our method in the BEAST software package (Suchard *et al.*, 2018), a popular tool for the study and reconstruction of rooted, time-measured phylogenies. We demonstrate the speed and accuracy of our linear-order gradient HMC versus previous best practices by examining the spread of the West Nile virus across the Americas in the early 2000s. Finally, we use our technique to apply the RRW model to study the sensitivity of correlation estimates to model misspecification between mammalian adult body mass and litter size across 2306 mammals, thereby demonstrating the scalability of our HMC implementation to tackling a previously intractable problem.

2 New Approaches

2.1 The Model

Consider a known or random phylogeny \mathcal{F} with N sampled tip nodes and $N - 1$ internal and root nodes, each with an observed or latent continuous trait value $\mathbf{Y}_i \in \mathbb{R}^P$. To traverse the phylogeny \mathcal{F} , let node $\text{pa}(i)$ index the parent of node i with branch length t_i connecting the two nodes. Then under the RRW model,

$$\mathbf{Y}_i \sim \text{MVN}(\mathbf{Y}_{\text{pa}(i)}, t_i \mathbf{V}(\phi_i)), \quad (1)$$

where the $P \times P$ matrix-valued function $\mathbf{V}(\phi_i)$ characterizes the branch-specific multivariate normal (MVN) increment that defines the diffusion process. We parameterize this function in terms of an unknown $P \times P$ positive-definite matrix Σ that describes the covariation between trait dimensions after controlling for shared evolutionary history and an unknown

branch-rate multiplier ϕ_i . Typical choices include

$$\mathbf{V}(\phi_i) = \begin{cases} \phi_i \mathbf{\Sigma} & \text{rate-scalar parameterization, } \phi_i > 0, \\ \frac{1}{\phi_i} \mathbf{\Sigma} & \text{scale-mixture-of-normals parameterization, } \phi_i > 0, \\ e^{\phi_i} \mathbf{\Sigma} & \text{unconstrained parameterization, and} \\ \mathbf{\Sigma} & \text{standard Brownian diffusion.} \end{cases} \quad (2)$$

To complete the RRW model specification, we adopt a prior density on the unobserved trait at the parentless root node,

$$p(\mathbf{Y}_{2N-1}) = \text{MVN}(\boldsymbol{\nu}_0, \kappa_0^{-1} \mathbf{\Sigma}) \quad (3)$$

with prior mean $\boldsymbol{\nu}_0$ and sample-size κ_0 .

Letting $\boldsymbol{\phi} = (\phi_1, \dots, \phi_{2N-2})$ and the observed data $\mathbf{Y} = (\mathbf{Y}_1, \dots, \mathbf{Y}_N)$ at the tips, we are interested in learning about the posterior

$$p(\boldsymbol{\phi}, \mathbf{\Sigma}, s, \mathcal{F}, \boldsymbol{\theta} \mid \mathbf{Y}, \mathbf{S}) \propto \underbrace{p(\mathbf{Y} \mid \boldsymbol{\phi}, \mathbf{\Sigma}, \mathcal{F})p(\mathbf{S} \mid \mathcal{F}, \boldsymbol{\theta})}_{\text{likelihood}} \underbrace{p(\boldsymbol{\phi} \mid s)p(s)p(\mathbf{\Sigma})p(\mathcal{F}, \boldsymbol{\theta})}_{\text{priors}}, \quad (4)$$

where s is an unknown parameter characterizing our prior on $\boldsymbol{\phi}$ and $\boldsymbol{\theta}$ represents parameters of a molecular sequence substitution model for the evolution of aligned molecular sequence data \mathbf{S} . Note that we follow usual convention (Cybis *et al.*, 2015) and assume that \mathbf{Y} and \mathbf{S} are conditionally independent given \mathcal{F} . We follow the example of Lemey *et al.* (2010) and place relatively uninformative priors on $\boldsymbol{\phi}$ and $\mathbf{\Sigma}$. For $\boldsymbol{\phi}$ we assign a log-normal prior distribution with mean 1 and standard deviation s and place an exponential prior on s . Additionally, we assign a Wishart conjugate prior with scale matrix \mathbf{I}_P and P degrees of freedom to $\mathbf{\Sigma}^{-1}$.

We use MCMC integration to approximate this posterior using a random-scan Metropolis-within-Gibbs approach (Levine and Casella, 2006; Liu, 2008). One cycle of this scheme consists of sampling $\boldsymbol{\phi}, \mathbf{\Sigma}, s$ and then $(\mathcal{F}, \boldsymbol{\theta})$ via

$$p(\boldsymbol{\phi} \mid \mathbf{\Sigma}, s, \mathcal{F}, \boldsymbol{\theta}, \mathbf{Y}, \mathbf{S}) \propto p(\mathbf{Y} \mid \boldsymbol{\phi}, \mathbf{\Sigma}, \mathcal{F})p(\boldsymbol{\phi} \mid s), \quad (5a)$$

$$p(\mathbf{\Sigma} \mid \boldsymbol{\phi}, s, \mathcal{F}, \boldsymbol{\theta}, \mathbf{Y}, \mathbf{S}) \propto p(\mathbf{Y} \mid \boldsymbol{\phi}, \mathbf{\Sigma}, \mathcal{F})p(\mathbf{\Sigma}), \quad (5b)$$

$$p(s \mid \boldsymbol{\phi}, \mathbf{\Sigma}, \mathcal{F}, \boldsymbol{\theta}, \mathbf{Y}, \mathbf{S}) \propto p(\boldsymbol{\phi} \mid s)p(s), \text{ and} \quad (5c)$$

$$p(\mathcal{F}, \boldsymbol{\theta} \mid \boldsymbol{\phi}, \mathbf{\Sigma}, s, \mathbf{Y}, \mathbf{S}) \propto p(\mathbf{Y} \mid \boldsymbol{\phi}, \mathbf{\Sigma}, \mathcal{F})p(\mathbf{S} \mid \mathcal{F}, \boldsymbol{\theta})p(\mathcal{F}, \boldsymbol{\theta}), \quad (5d)$$

where update (5d) is unnecessary when \mathcal{F} is fixed, otherwise efficient sampling from the density $p(\mathcal{F}, \boldsymbol{\theta} \mid \boldsymbol{\phi}, \mathbf{\Sigma}, s, \mathbf{Y}, \mathbf{S})$ is well described elsewhere, see for example Suchard *et al.* (2018). Updates (5b) and (5c) are straightforward due to the conjugate priors chosen in our model. We turn our focus to the remaining component of our scheme, namely sampling from $p(\boldsymbol{\phi} \mid \mathbf{\Sigma}, s, \mathcal{F}, \boldsymbol{\theta}, \mathbf{Y}, \mathbf{S})$.

2.2 Hamiltonian Monte Carlo

We wish to sample $\boldsymbol{\phi}$ jointly to avoid potentially high autocorrelation in the resulting MCMC chain. To this end, we propose using HMC and begin with a brief description of how HMC

maps sampling from a probability distribution to simulating a physical system. In classical mechanics, the Hamiltonian is the sum of the kinetic and potential energy in a closed system. To build the connection, we introduce auxiliary momentum variable $\boldsymbol{\rho} = (\rho_1, \dots, \rho_{2N-2})$ and write our Hamiltonian,

$$H(\boldsymbol{\phi}, \boldsymbol{\rho}) = \underbrace{-\log p(\boldsymbol{\phi} | \boldsymbol{\Sigma}, s, \mathcal{F}, \boldsymbol{\theta}, \mathbf{Y}, \mathbf{S})}_{\text{potential energy}} + \underbrace{\frac{1}{2} \boldsymbol{\rho}^t \mathbf{M} \boldsymbol{\rho}}_{\text{kinetic energy}}, \quad (6)$$

where the mass matrix \mathbf{M} weights our momentum variables. The canonical distribution from statistical mechanics relates the joint density of state variables $\boldsymbol{\phi}$ and $\boldsymbol{\rho}$ to the energy in a system via the relationship,

$$p(\boldsymbol{\phi}, \boldsymbol{\rho} | \boldsymbol{\Sigma}, s, \mathcal{F}, \boldsymbol{\theta}, \mathbf{Y}, \mathbf{S}) \propto e^{-H(\boldsymbol{\phi}, \boldsymbol{\rho})}. \quad (7)$$

Substituting our Hamiltonian into (7), we observe that $\boldsymbol{\phi}$ and $\boldsymbol{\rho}$ are independent and recognize the marginal density of $\boldsymbol{\rho}$ to be MVN. To start the HMC algorithm, we first sample $\boldsymbol{\rho}$ from this marginal density. Then by differentiating $H(\boldsymbol{\phi}, \boldsymbol{\rho})$, we generate Hamilton's equations of motion,

$$\begin{aligned} \frac{d\phi_i}{dt} &= +\frac{\partial H}{\partial \rho_i}, \text{ and} \\ \frac{d\rho_i}{dt} &= -\frac{\partial H}{\partial \phi_i} = \frac{\partial}{\partial \phi_i} \log p(\boldsymbol{\phi} | \boldsymbol{\Sigma}, s, \mathcal{F}, \boldsymbol{\theta}, \mathbf{Y}, \mathbf{S}) \text{ for all } i = 1, \dots, 2N-2. \end{aligned} \quad (8)$$

We can use the resulting vector field in conjunction with a variety of numerical integration techniques to propose new states of $\boldsymbol{\phi}$ for our MCMC chain. Consistent with typical construction (Neal, 2011), we use the leapfrog method for numerical integration, where we follow the trajectory of $\boldsymbol{\rho}$ for a half-step before updating $\boldsymbol{\phi}$. For a full discussion of HMC, see Neal (2011). Importantly, Hamilton's equations elicit a need to calculate $\nabla_{\boldsymbol{\phi}} \log p(\boldsymbol{\phi} | \boldsymbol{\Sigma}, s, \mathcal{F}, \boldsymbol{\theta}, \mathbf{Y}, \mathbf{S}) = \left(\frac{\partial}{\partial \phi_1}, \dots, \frac{\partial}{\partial \phi_{2N-2}} \right)^t \log p(\boldsymbol{\phi} | \boldsymbol{\Sigma}, s, \mathcal{F}, \boldsymbol{\theta}, \mathbf{Y}, \mathbf{S})$ to traverse phase space.

2.3 Gradient of trait data log-likelihood

A practical HMC sampler demands efficient calculation of $\nabla_{\boldsymbol{\phi}} \log p(\boldsymbol{\phi} | \boldsymbol{\Sigma}, s, \mathcal{F}, \boldsymbol{\theta}, \mathbf{Y}, \mathbf{S})$. Differentiating the logarithm of (5a), we obtain

$$\frac{\partial}{\partial \phi_i} \log p(\boldsymbol{\phi} | \boldsymbol{\Sigma}, s, \mathcal{F}, \mathbf{Y}, \mathbf{S}) = \frac{\partial}{\partial \phi_i} \log p(\mathbf{Y} | \boldsymbol{\phi}, \boldsymbol{\Sigma}, \mathcal{F}) + \frac{\partial}{\partial \phi_i} \log p(\boldsymbol{\phi} | s). \quad (9)$$

We choose a log-normal prior for $\boldsymbol{\phi}$ and so evaluating the second term in Equation (9) is trivial. Indeed, this term remains trivial for many common priors one might choose for $\boldsymbol{\phi}$. Here we develop a general recursive algorithm for calculating $\nabla_{\boldsymbol{\phi}} \log p(\mathbf{Y} | \boldsymbol{\phi}, \boldsymbol{\Sigma}, \mathcal{F})$. To facilitate this development, consider splitting \mathbf{Y} into two disjoint sets relative to any node i in \mathcal{F} . We define $\mathbf{Y}_{[i]}$ as the observed data descendant of node i and $\mathbf{Y}_{[i]}$ as the observed data “above” (or not descendent of) node i . For clarity, see Figure (1).

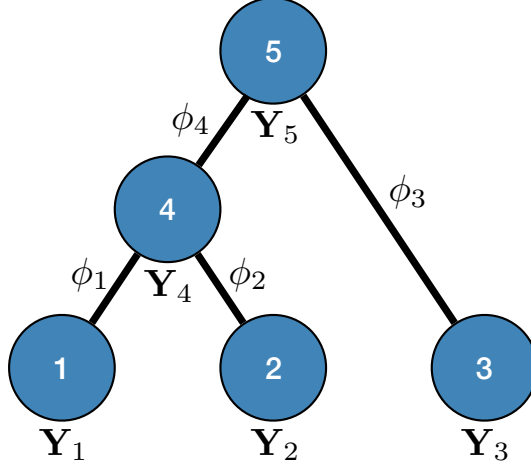


Figure 1: Example tree with $N = 3$ tips. Assume trait data \mathbf{Y}_i are fully observed for $i = \{1, 2, 3\}$. We write $\mathbf{Y}_{[4]}$ and $\mathbf{Y}_{\lceil 4 \rceil}$ to denote the observed data below and above node 4 respectively. Specifically, $\mathbf{Y}_{[4]} = \{\mathbf{Y}_1, \mathbf{Y}_2\}$ while $\mathbf{Y}_{\lceil 4 \rceil} = \{\mathbf{Y}_3\}$. Partial likelihoods $p(\mathbf{Y}_{[4]} | \mathbf{Y}_4) = p(\mathbf{Y}_1, \mathbf{Y}_2 | \mathbf{Y}_4)$ and $p(\mathbf{Y}_4 | \mathbf{Y}_{\lceil 4 \rceil}) = p(\mathbf{Y}_4 | \mathbf{Y}_3)$.

In the following, we drop the dependence of the log-likelihood on ϕ , Σ and \mathcal{F} for notational convenience. To begin,

$$\begin{aligned}
\frac{\partial}{\partial \phi_i} [\log p(\mathbf{Y})] &= \frac{\partial}{\partial \phi_i} [p(\mathbf{Y})] / p(\mathbf{Y}) \\
&= \frac{\partial}{\partial \phi_i} \left[\int p(\mathbf{Y}_{[i]} | \mathbf{Y}_i) p(\mathbf{Y}_i | \mathbf{Y}_{\lceil i \rceil}) p(\mathbf{Y}_{\lceil i \rceil}) d\mathbf{Y}_i / p(\mathbf{Y}) \right] \\
&= \int \frac{\partial}{\partial \phi_i} [p(\mathbf{Y}_{[i]} | \mathbf{Y}_i) p(\mathbf{Y}_i | \mathbf{Y}_{\lceil i \rceil}) p(\mathbf{Y}_{\lceil i \rceil})] d\mathbf{Y}_i / p(\mathbf{Y}) \\
&= \int p(\mathbf{Y}_{[i]} | \mathbf{Y}_i) \frac{\partial}{\partial \phi_i} [p(\mathbf{Y}_i | \mathbf{Y}_{\lceil i \rceil})] p(\mathbf{Y}_{\lceil i \rceil}) d\mathbf{Y}_i / p(\mathbf{Y}).
\end{aligned} \tag{10}$$

The last equality above follows from the fact that ϕ_i is associated only with the branch above node i . Therefore when we condition on \mathbf{Y}_i , $\mathbf{Y}_{[i]}$ is independent of ϕ_i . Similarly, $\mathbf{Y}_{\lceil i \rceil}$ evolves independent of ϕ_i . To proceed with the differential above, we use the fact that $p(\mathbf{Y}_i | \mathbf{Y}_{\lceil i \rceil})$ follows a MVN distribution with as of yet undetermined mean \mathbf{n}_i and precision \mathbf{Q}_i (see section (6.3) for a detailed derivation). We extract the middle term from Equation (10) and find

$$\begin{aligned}
\frac{\partial}{\partial \phi_i} [p(\mathbf{Y}_i | \mathbf{Y}_{\lceil i \rceil})] &= \frac{1}{2} \left\{ (\mathbf{Y}_i - \mathbf{n}_i)^t \mathbf{Q}_i t_i \frac{\partial}{\partial \phi_i} [\mathbf{V}(\phi_i)] \mathbf{Q}_i (\mathbf{Y}_i - \mathbf{n}_i) \right. \\
&\quad \left. - \text{tr} \left[\mathbf{Q}_i t_i \frac{\partial}{\partial \phi_i} [\mathbf{V}(\phi_i)] \right] \right\} p(\mathbf{Y}_i | \mathbf{Y}_{\lceil i \rceil}),
\end{aligned} \tag{11}$$

using the differential properties

$$\begin{aligned}
d\mathbf{Q}_i &= -\mathbf{Q}_i (d\mathbf{Q}_i^{-1}) \mathbf{Q}_i \text{ and} \\
d|\mathbf{Q}_i^{-1}| &= |\mathbf{Q}_i^{-1}| \text{tr} [\mathbf{Q}_i d\mathbf{Q}_i^{-1}],
\end{aligned} \tag{12}$$

found in, e.g., [Petersen *et al.* \(2008\)](#).

To simplify notation, we let function

$$\mathbf{F}(\mathbf{Y}_i) = \frac{1}{2} \{ (\mathbf{Y}_i - \mathbf{n}_i)^t \boldsymbol{\Upsilon}_i (\mathbf{Y}_i - \mathbf{n}_i) - \text{tr}[\boldsymbol{\chi}_i] \}, \quad (13)$$

where $\boldsymbol{\Upsilon}_i = \mathbf{Q}_i t_i \frac{\partial}{\partial \phi_i} [\mathbf{V}(\phi_i)] \mathbf{Q}_i$ and $\boldsymbol{\chi}_i = \mathbf{Q}_i t_i \frac{\partial}{\partial \phi_i} [\mathbf{V}(\phi_i)]$. Substituting Equation (13) back into Equation (10), we observe that

$$\begin{aligned} \frac{\partial}{\partial \phi_i} [\log p(\mathbf{Y})] &= \int \mathbf{F}(\mathbf{Y}_i) p(\mathbf{Y}_{[i]} | \mathbf{Y}_i) p(\mathbf{Y}_i | \mathbf{Y}_{[i]}) p(\mathbf{Y}_{[i]}) d\mathbf{Y}_i / p(\mathbf{Y}) \\ &= \int \mathbf{F}(\mathbf{Y}_i) p(\mathbf{Y}_i | \mathbf{Y}) d\mathbf{Y}_i \\ &= \mathbb{E}[\mathbf{F}(\mathbf{Y}_i) | \mathbf{Y}]. \end{aligned} \quad (14)$$

When \mathbf{Y}_i is fully observed (typically $i \leq N$), this expectation collapses to the direct evaluation of $\mathbf{F}(\mathbf{Y}_i)$. When $i = N+1, \dots, 2N-2$ or if \mathbf{Y}_i is partially observed for $i = 1, \dots, N$, we require $p(\mathbf{Y}_i | \mathbf{Y})$. From Bayes' theorem, $p(\mathbf{Y}_i | \mathbf{Y}) \propto p(\mathbf{Y}_{[i]} | \mathbf{Y}_i) p(\mathbf{Y}_i | \mathbf{Y}_{[i]})$. Partial likelihood $p(\mathbf{Y}_{[i]} | \mathbf{Y}_i)$ is proportional to a MVN density characterized by computable mean \mathbf{m}_i and precision \mathbf{P}_i ([Pybus *et al.*, 2012](#)). Using this fact, $p(\mathbf{Y}_i | \mathbf{Y})$ becomes MVN with mean $\boldsymbol{\mu}_i = \mathbf{Z}_i (\mathbf{P}_i \mathbf{m}_i + \mathbf{Q}_i \mathbf{n}_i)$ and variance $\mathbf{Z}_i = [\mathbf{P}_i + \mathbf{Q}_i]^{-1}$. Finally,

$$\mathbb{E}[\mathbf{F}(\mathbf{Y}_i) | \mathbf{Y}_1, \dots, \mathbf{Y}_N] = \frac{1}{2} \{ \text{tr}[\mathbf{Z}_i \boldsymbol{\Upsilon}_i] + (\boldsymbol{\mu}_i - \mathbf{n}_i)^t \boldsymbol{\Upsilon}_i (\boldsymbol{\mu}_i - \mathbf{n}_i) - \text{tr}[\boldsymbol{\chi}_i] \}. \quad (15)$$

Equation (15) provides a recipe to compute $\nabla_{\phi} \log p(\mathbf{Y} | \phi, \boldsymbol{\Sigma}, \mathcal{F})$ using the means and precisions that characterize partial data likelihoods $p(\mathbf{Y}_i | \mathbf{Y}_{[i]})$ and $p(\mathbf{Y}_{[i]} | \mathbf{Y}_i)$.

2.4 Tree Traversals

We introduce post- and pre-order tree traversals to recursively calculate all partial data likelihood means and precisions in computational complexity $\mathcal{O}(N)$ that scales linearly with N . To begin, let nodes i and j be daughters of node k . For the post-order traversal,

$$p(\mathbf{Y}_{[i]} | \mathbf{Y}_i) \propto \text{MVN}(\mathbf{Y}_i; \mathbf{m}_i, \mathbf{P}_i^{-1}), \quad (16)$$

with post-order mean \mathbf{m}_i and precision \mathbf{P}_i . For $k = 1, \dots, 2N-1$ in post-order, we build the inverse-precision (variance) via

$$\mathbf{P}_k^{-1} = \begin{cases} 0 \times \mathbf{I} & \text{if } k \text{ is a tip} \\ (\mathbf{P}_i^* + \mathbf{P}_j^*)^{-1} & \text{otherwise,} \end{cases} \quad (17)$$

where

$$\mathbf{P}_i^* = \left(\mathbf{P}_i^{-1} + t_i \mathbf{V}(\phi_i) \right)^{-1} \quad \text{and} \quad \mathbf{P}_j^* = \left(\mathbf{P}_j^{-1} + t_j \mathbf{V}(\phi_j) \right)^{-1} \quad (18)$$

and the mean via

$$\mathbf{m}_k = \begin{cases} \mathbf{Y}_k & \text{if } k \text{ is a tip} \\ \mathbf{P}_k^{-1} (\mathbf{P}_i^* \mathbf{m}_i + \mathbf{P}_j^* \mathbf{m}_j) & \text{otherwise.} \end{cases} \quad (19)$$

For a proof of these post-order updates, see [Pybus *et al.* \(2012\)](#) (Supplemental Material).

To compute $p(\mathbf{Y}_i | \mathbf{Y}_{[i]})$, we traverse the tree in pre-order fashion according to our generalized version of the recursive algorithm proposed by [Cybis *et al.* \(2015\)](#). See section (6.3) for a derivation of our generalized pre-order update. For the pre-order traversal,

$$p(\mathbf{Y}_i | \mathbf{Y}_{[i]}) = \text{MVN}(\mathbf{Y}_i; \mathbf{n}_i, \mathbf{Q}_i^{-1}). \quad (20)$$

For $i = 2N - 1, \dots, 1$ looking down the tree, we update our pre-order precision,

$$\mathbf{Q}_i = \begin{cases} \kappa_0 \mathbf{\Sigma}^{-1} & \text{if } i \text{ is root} \\ \left((\mathbf{Q}_i^*)^{-1} + t_i \mathbf{V}(\phi_i) \right)^{-1} & \text{otherwise} \end{cases} \quad (21)$$

at each node where

$$\mathbf{Q}_i^* = \mathbf{P}_j^* + \mathbf{Q}_k. \quad (22)$$

We also keep track of the pre-order mean at each node via

$$\mathbf{n}_i = \begin{cases} \nu_0 & \text{if } i \text{ is root} \\ (\mathbf{Q}_i^*)^{-1} (\mathbf{P}_j^* \mathbf{m}_j + \mathbf{Q}_k \mathbf{n}_k) & \text{otherwise.} \end{cases} \quad (23)$$

Both traversals visit each node exactly once and perform a matrix inversion as their most costly operation, providing an $\mathcal{O}(NP^3)$ algorithm. However, as we observe in Equation (2), generally $\mathbf{V}(\phi_i) = g(\phi_i) \mathbf{\Sigma}$. In this case, we can further reduce the computational complexity to $\mathcal{O}(NP^2)$ by factoring out $\mathbf{\Sigma}$. Instead of inverting $\mathbf{V}(\phi_i)$ at each step, we only need to invert $\mathbf{\Sigma}$ at most once per likelihood or gradient evaluation.

3 Results

3.1 West Nile Virus

West Nile virus (WNV) is responsible for more than 1,500 deaths and caused over 700,000 illnesses since first reported in North America in 1999. The virus typically spreads via mosquito bites; however, the primary host is birds. First identified in New York City, WNV spread to the Pacific coast by 2003 and reached south into Argentina by 2005 ([Petersen *et al.*, 2013](#)). We examine whole aligned viral genomes (11,029 nt) and geographic data on 104 cases of WNV collected between 1999 and 2007 ([Pybus *et al.*, 2012](#)). In cases where only the year of sampling is known, we set the sampling date to the midpoint of that year. Previous authors have recorded latitude and longitude geographic sampling information by converting zip code locations using ZIPList5. For 27 of the specimens, only the U.S. or Mexican state of discovery is known and so we have augmented sampling data with the coordinates of the centroid of the state ([Pybus *et al.*, 2012](#)).

Here we study the simultaneous evolution and dispersal of WNV as it spreads across North America, following the modeling choices of [Pybus *et al.* \(2012\)](#). We define geographic location as our trait of interest \mathbf{Y} within a RRW and infer rates ϕ using our new HMC method. We compare the computational efficiency of our method to the random-scan UMH approach employed by [Pybus *et al.* \(2012\)](#). We use effective sample size (ESS) of the posterior

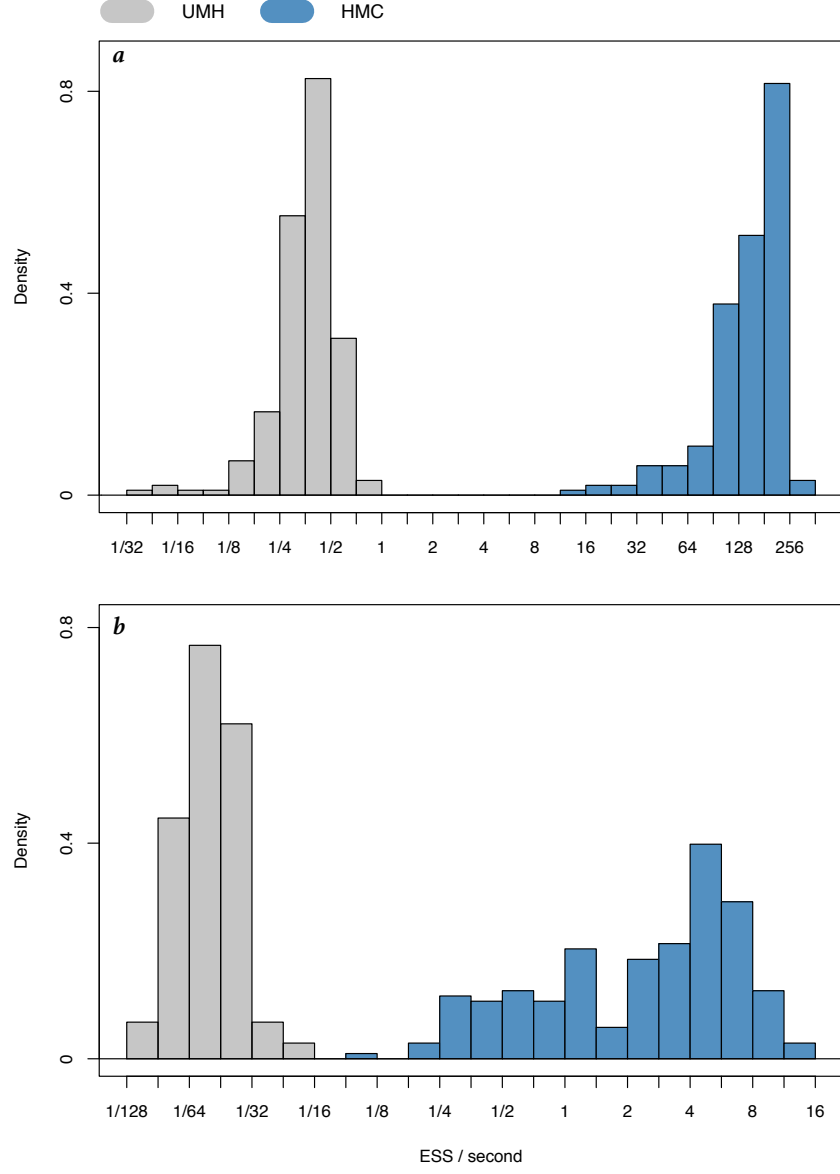


Figure 2: Comparing computational efficiency of Hamiltonian Monte Carlo (HMC) and univariable Metropolis-Hastings (UMH) transition kernels through effective sample size (ESS) per unit time in West Nile virus (WNV) phylogeography. **(a)**: Fixed phylogeny \mathcal{F} , diffusion matrix Σ and prior standard deviation s . **(b)**: Inference on the full joint posterior, $p(\phi, s, \Sigma, \mathcal{F}, \theta | \mathbf{Y}, \mathbf{S})$.

ϕ_i samples for all i divided by computational runtime to evaluate the performance of each MCMC approach. Specifically, we report ESS/second for two separate inference cases. In case (a) we fix standard deviation s of the prior $p(\phi | s)$ as well as diffusion matrix Σ and phylogeny \mathcal{F} to posterior mean estimates of these values (see section (6)) and strictly sample ϕ . In case (b) we perform simultaneous inference on all parameters of the full posterior (4). Because BEAST employs a random-scan approach across model parameters, we adjust the weight of our HMC transition kernel so that the proportion of time spent sampling branch-rate multiplier space with HMC equals the proportion of time spent with UMH. We report histograms of ESS/second in both cases across all branches in Figure (2).

In case (a) the median ESS/second across ϕ is 164 and 0.374 for the HMC and UMH transition kernels respectively. This demonstrates a 439-fold speed increase. Additionally, the minimum ESS/second is 14.3 with HMC and 0.038 with UMH, exhibiting a 375-fold speed-up for the “least well” explored ϕ_i . In case (b), the median ESS/second is 3.08 and 0.019 for the HMC and UMH transition kernels respectively, exhibiting a 162-fold speed-up while controlling for proportion of time spent in each transition kernel. The ratio of minimum speed-up in case (b) is 15.3, however the “least well” explored dimensions are multimodal possibly due to the lack of identifiability among some branch-rate multipliers induced by the non-constant nature of the phylogeny.

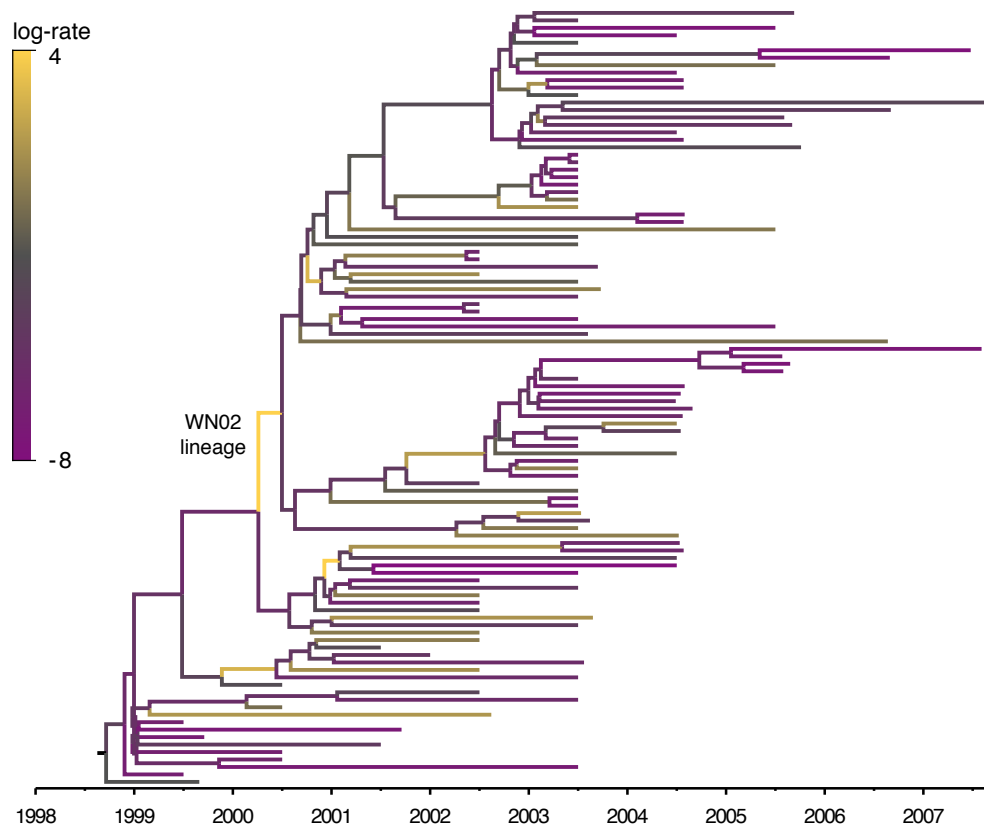


Figure 3: Maximum clade credible (MCC) tree resulting from Hamiltonian Monte Carlo (HMC) inference under phylogeographic relaxed random walk (RRW) of West Nile virus. We color branches by posterior mean branch-rate parameters ϕ .

In Figure (3) we report the maximum clade credible (MCC) tree, obtained from applying HMC to the RRW model as described in case (b), where substitution rate variation is accounted for by the molecular clock model (see 6). The branch with the highest posterior dispersal rate starts the WN02 lineage identified by Gray *et al.* (2010). The clade of New York isolates sampled in 1999, however, maintains a much slower dispersal rate. Sufficiently precise posterior estimates under the previous UMH approach remain unavailable in reasonable time to expose these differences.

3.2 Mammalian Life History

Life history theory aims to explain how traits such as adult body mass, litter size and lifespan evolve to optimize reproductive success (Stearns, 2000). To understand how diversity is maintained in life history traits in the presence of evolutionary forces, it is important to understand how they covary. In mammals, adult body mass exhibits weak negative correlation with litter size (Sikes and Ylönen, 1998) but this conclusion may be an artifact of the restrictive assumptions of strict Brownian diffusion modeling. Here we re-evaluate this claim with the RRW of trait evolution made tractable through $\mathcal{O}(N)$ HMC sampling.

Under the RRW, we infer correlation between adult body mass and litter size from the PanTHERIA data set (Jones *et al.*, 2009) across 2306 mammalian species related by the fixed supertree of Fritz *et al.* (2009). After log-transforming and standardizing the trait measurements, we estimate a posterior mean correlation between adult body mass and litter size of -3.64×10^{-2} , with 95% high posterior density (HPD) interval $\{-8.62 \times 10^{-2}, 1.37 \times 10^{-2}\}$. This finding remains consistent with the hypothesis that there exists weak negative correlation. To gauge the effect of a heterogeneous diffusion process on the correlation between traits, we also make inference using the strict Brownian diffusion model where the ϕ are all identically 1. Here, we find the correlation between traits to be -3.37×10^{-2} $\{-7.45 \times 10^{-2}, 6.91 \times 10^{-3}\}$. The HPD intervals are similar under both models and indeed the estimated probability that the correlation is <0 is 0.93 under the RRW model and 0.94 under the strict Brownian diffusion model. In this case, our generalized model reassuringly confirms the previous analysis under the more limited model. We report a density plot of inferred diffusion matrix Σ in Figure (4).

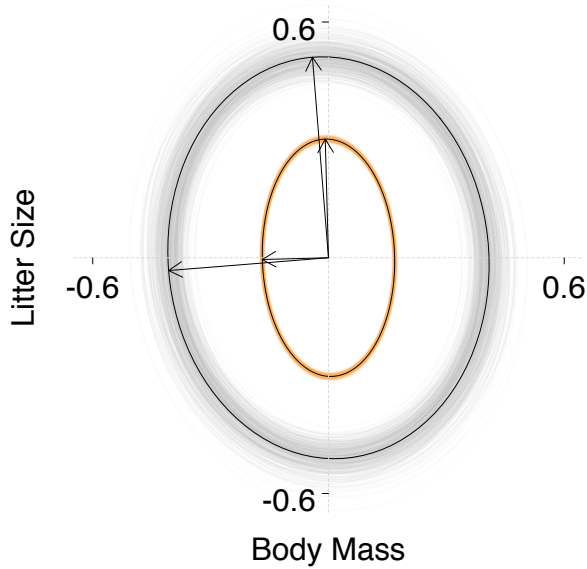


Figure 4: Posterior density of diffusion matrix Σ relating mammalian body mass to litter size. We plot solutions of $Y^t \Sigma^{-1} Y = c$ where we choose c such that the ellipses trace 95% of the multivariate normal (MVN) mass. We log transform and standardize traits before inference of Σ . The gray rings depict estimates under the relaxed random walk (RRW) model while the orange contours represent estimates under the strict Brownian diffusion model. The black rings show the posterior mean Σ under each model and the vectors are principal axes of these posterior mean ellipsoids.

4 Discussion

Previous MCMC techniques to investigate trait evolution under the RRW model scale poorly with large data sets. Specifically the UMH transition kernel is ineffective for sampling correlated, high dimensional parameter space. We provide a remedy by using an HMC transition kernel to sample all branch-rate multipliers simultaneously. To improve the speed of HMC we derive an algorithm for calculating the gradient of the trait data log-likelihood. Our gradient calculation achieves $\mathcal{O}(N)$ computational speed, a vast improvement compared to both numerical and pruning methods for calculating the gradient that typically require $\mathcal{O}(N^2)$.

We observe over 300-fold speed-up when comparing our HMC transition kernel to UMH in the spread of the WNV across North America in the early 2000s. The resulting MCC tree reveals that the largest rate of dispersion precedes the most recent common ancestor of the WN02 lineage. Subsequently, the rates of dispersion slow down through the WN02 clade. This suggests that this clade developed after some rapid geographic displacement. Interestingly, the appearance of smaller branch-rate multipliers within the WN02 lineage is consistent with the slowing speed of sequence evolution as described in [Snapinn *et al.* \(2007\)](#).

As exhibited in Figure (2), ESS from posterior sampling accumulates at variable speed

across the branches of the tree. To further improve the sampling of our HMC algorithm, one might use an approximation of the posterior covariance of ϕ for the mass matrix \mathbf{M} to appropriately weight momentum updates in the HMC algorithm (Neal, 2011). Possible approximations include the Hessian of the log-posterior (a local approximation of the curvature of branch-rate multiplier space) or the sample variance across each dimension. An important consideration in choosing an appropriate \mathbf{M} is whether one is studying under a fixed or random phylogeny \mathcal{F} . Since varying \mathcal{F} in the posterior often creates multimodal distributions of ϕ , local approximations such as the Hessian may be of limited assistance in such cases.

We show in our application to mammalian life history that our computationally efficient HMC algorithm imbues the RRW model with the ability to handle large trees with thousands of taxa. Applying the RRW model to this massive example allows us to confirm the existence of weak negative correlation between body mass and litter size as exhibited by the principle axes of Figure (4). Furthermore, we observe that the variability in body mass is modestly greater than the variability in litter size and this phenomenon is present under both models of trait evolution.

In a time where biological data are larger and more prolific than ever, scalable approaches to complex models of evolution such as the RRW prove increasingly useful in a variety of applications. From spatial epidemiology where determining the dispersal rate of an infectious disease is crucial, to evolutionary ecology where an organism’s fitness is determined by the covariability across life history traits, the need for computationally faster approaches stands evident. We hope that this work will serve to improve the speed of such analyses.

5 Acknowledgments

This work was supported by the European Research Council under the European Union’s Horizon 2020 research and innovation programme (grant agreement number 725422 - ReservoirDOCS); The Artic Network from the Wellcome Trust (grant number 206298/Z/17/Z); National Science Foundation (grant number DMS 1264153); National Institutes of Health (grants R01 AI107034, U19 AI135995, and T32 GM008185 to AAF); and Research Foundation – Flanders (‘Fonds voor Wetenschappelijk Onderzoek – Vlaanderen’, G066215N, G0D5117N and G0B9317N) to PL.

6 Materials and Methods

6.1 West Nile Virus

In the WNV application, we first follow Pybus *et al.* (2012) by employing a RRW model with log-normal prior on rates ϕ with mean = 1 and standard deviation s and use a general time-reversible (GTR) + Γ substitution model with a log-normal relaxed molecular clock. We use the UMH transition kernel for a 250 million state MCMC chain simulation. Subsequently, we use the resulting posterior mean estimates of Σ and s , as well as the MCC tree to fix these model parameters in the analysis of case (a) described in our work here. Under this fixed analysis we run our HMC-based chain for 1 million states and a UMH-based chain for

150 million states. In case (b), we use a random starting tree and jointly estimated ϕ , Σ , s , \mathcal{F} and θ . We simulate MCMC chains for 25 million and 250 million states using HMC and UMH transition kernels respectively.

6.2 Mammalian Life History

For the mammalian life history application, we examine two models of trait evolution along a fixed phylogeny. Under the RRW, we jointly infer ϕ , Σ and s , running our HMC-based chain for 1 million states. Under the strict Brownian diffusion model, we perform MCMC inference on the diffusion matrix Σ for 1 million states.

6.3 Pre-Order Partial Likelihood

In this section we derive a generalized version of the pre-order recursive algorithm proposed by Cybis *et al.* (2015) to compute $p(\mathbf{Y}_i | \mathbf{Y}_{[i]})$ for all i in $\mathcal{O}(N)$. We begin with the law of total probability,

$$p(\mathbf{Y}_i | \mathbf{Y}_{[i]}) \propto \int p(\mathbf{Y}_i | \mathbf{Y}_k) p(\mathbf{Y}_{[j]} | \mathbf{Y}_k) p(\mathbf{Y}_k | \mathbf{Y}_{[k]}) d\mathbf{Y}_k \quad (24)$$

for node i with parent k and sibling j . Recalling that

$$\begin{aligned} p(\mathbf{Y}_i | \mathbf{Y}_k) &= \text{MVN}(\mathbf{Y}_i; \mathbf{Y}_k, t_i \mathbf{V}(\phi_i)), \text{ and} \\ p(\mathbf{Y}_{[j]} | \mathbf{Y}_k) &\propto \text{MVN}(\mathbf{Y}_k; \mathbf{m}_j, (\mathbf{P}_j^*)^{-1}), \end{aligned} \quad (25)$$

we identify Equation (24) as a recursive expression whose solution has the form

$$p(\mathbf{Y}_i | \mathbf{Y}_{[i]}) = \text{MVN}(\mathbf{Y}_i; \mathbf{n}_i, \mathbf{Q}_i^{-1}), \quad (26)$$

with presently undetermined pre-order mean \mathbf{n}_i and pre-order precision \mathbf{Q}_i .

We unravel these quantities by first identifying that $p(\mathbf{Y}_{2N-1} | \mathbf{Y}_{[2N-1]}) = p(\mathbf{Y}_{2N-1})$ and set $\mathbf{n}_{2N-1} = \nu_0$ and $\mathbf{Q}_{2N-1} = \kappa_0 \Sigma^{-1}$. Then proceeding in pre-order fashion for $i = 2N-2, \dots, 1$

$$\begin{aligned} \mathbf{Q}_i &= \left((\mathbf{Q}_i^*)^{-1} + t_i \mathbf{V}(\phi_i) \right)^{-1} \text{ where} \\ \mathbf{Q}_i^* &= \mathbf{P}_j^* + \mathbf{Q}_k, \text{ and} \\ \mathbf{n}_i &= (\mathbf{Q}_i^*)^{-1} (\mathbf{P}_j^* \mathbf{m}_j + \mathbf{Q}_k \mathbf{n}_k). \end{aligned} \quad (27)$$

Bibliography

- Bedford, T., Suchard, M. A., Lemey, P., Dudas, G., Gregory, V., Hay, A. J., McCauley, J. W., Russell, C. A., Smith, D. J., and Rambaut, A. (2014). Integrating influenza antigenic dynamics with molecular evolution. *eLife*, **3**, e01914.
- Betancourt, M. (2017). unpublished data. A conceptual introduction to Hamiltonian Monte Carlo, <https://arxiv.org/abs/1701.02434>, last accessed May 31, 2019.

- Biek, R., Henderson, J. C., Waller, L. A., Rupprecht, C. E., and Real, L. A. (2007). A high-resolution genetic signature of demographic and spatial expansion in epizootic rabies virus. *Proceedings of the National Academy of Sciences*, **104**(19), 7993–7998.
- Bryant, D., Galtier, N., and Poursat, M.-A. (2005). Likelihood calculation in molecular phylogenetics. In O. Gascuel, editor, *Mathematics of Evolution and Phylogeny*, pages 33–62. Oxford Univ. Press.
- Cybis, G. B., Sinsheimer, J. S., Bedford, T., Mather, A. E., Lemey, P., and Suchard, M. A. (2015). Assessing phenotypic correlation through the multivariate phylogenetic latent liability model. *The Annals of Applied Statistics*, **9**(2), 969.
- Faria, N. R., Rambaut, A., Suchard, M. A., Baele, G., Bedford, T., Ward, M. J., Tatem, A. J., Sousa, J. D., Arinaminpathy, N., P  pin, J., *et al.* (2014). The early spread and epidemic ignition of HIV-1 in human populations. *Science*, **346**(6205), 56–61.
- Felsenstein, J. (1981). Evolutionary trees from DNA sequences: a maximum likelihood approach. *Journal of Molecular Evolution*, **17**(6), 368–376.
- Felsenstein, J. (1985). Phylogenies and the comparative method. *The American Naturalist*, **125**(1), 1–15.
- Fritz, S. A., Bininda-Emonds, O. R., and Purvis, A. (2009). Geographical variation in predictors of mammalian extinction risk: big is bad, but only in the tropics. *Ecology Letters*, **12**(6), 538–549.
- Gray, R., Veras, N., Santos, L., and Salemi, M. (2010). Evolutionary characterization of the West Nile virus complete genome. *Molecular Phylogenetics and Evolution*, **56**(1), 195–200.
- Hastings, W. K. (1970). Monte Carlo sampling methods using Markov chains and their applications. *Biometrika*, **57**(1), 97 – 109.
- Ives, A. R. and Garland Jr, T. (2009). Phylogenetic logistic regression for binary dependent variables. *Systematic Biology*, **59**(1), 9–26.
- Jones, K. E., Bielby, J., Cardillo, M., Fritz, S. A., O’Dell, J., Orme, C. D. L., Safi, K., Sechrest, W., Boakes, E. H., Carbone, C., *et al.* (2009). PanTHERIA: a species-level database of life history, ecology, and geography of extant and recently extinct mammals. *Ecology*, **90**(9), 2648–2648.
- Lemey, P., Rambaut, A., Welch, J. J., and Suchard, M. A. (2010). Phylogeography takes a relaxed random walk in continuous space and time. *Molecular Biology and Evolution*, **27**(8), 1877–1885.
- Levine, R. A. and Casella, G. (2006). Optimizing random scan Gibbs samplers. *Journal of Multivariate Analysis*, **97**(10), 2071–2100.
- Liu, J. S. (2008). *Monte Carlo strategies in scientific computing*. Springer Science & Business Media.

- Neal, R. M. (2011). MCMC using Hamiltonian dynamics. In S. Brooks, A. Gelman, G. L. Jones, and X.-L. Meng, editors, *Handbook of Markov Chain Monte Carlo*, volume 2. CRC Press New York, NY.
- Petersen, K. B., Pedersen, M. S., *et al.* (2008). The matrix cookbook. *Technical University of Denmark*, **7**(15), 510.
- Petersen, L. R., Brault, A. C., and Nasci, R. S. (2013). West Nile virus: review of the literature. *Journal of the American Medical Association*, **310**(3), 308–315.
- Pybus, O. G., Suchard, M. A., Lemey, P., Bernardin, F. J., Rambaut, A., Crawford, F. W., Gray, R. R., Arinaminpathy, N., Stramer, S. L., Busch, M. P., *et al.* (2012). Unifying the spatial epidemiology and molecular evolution of emerging epidemics. *Proceedings of the National Academy of Sciences*, **109**(37), 15066–15071.
- Schluter, D., Price, T., Mooers, A. Ø., and Ludwig, D. (1997). Likelihood of ancestor states in adaptive radiation. *Evolution*, **51**(6), 1699–1711.
- Sikes, R. S. and Ylönen, H. (1998). Considerations of optimal litter size in mammals. *Oikos*, **83**(3), 452–465.
- Snapinn, K. W., Holmes, E. C., Young, D. S., Bernard, K. A., Kramer, L. D., and Ebel, G. D. (2007). Declining growth rate of West Nile virus in North America. *Journal of Virology*, **81**(5), 2531–2534.
- Stearns, S. C. (2000). Life history evolution: successes, limitations, and prospects. *Naturwissenschaften*, **87**(11), 476–486.
- Suchard, M. A., Lemey, P., Baele, G., Ayres, D. L., Drummond, A. J., and Rambaut, A. (2018). Bayesian phylogenetic and phylodynamic data integration using BEAST 1.10. *Virus Evolution*, **4**(1), vey016.